

UNCLASSIFIED

AD NUMBER

AD801718

NEW LIMITATION CHANGE

TO

**Approved for public release, distribution
unlimited**

FROM

**Distribution authorized to U.S. Gov't.
agencies and their contractors; Critical
Technology; 03 DEC 1958. Other requests
shall be referred to Space and Missile
System, Los Angeles, CA.**

AUTHORITY

SAMSO USAF ltr, 28 Feb 1972

THIS PAGE IS UNCLASSIFIED

LMSD
5151

C3P

SHELF LISTED

801718

LMSD-5151

3 DECEMBER 1958

LMSD LIBRARY INVENTORY - PALO ALTO
Return to LMSC Library. Do not destroy
or transmit to another person or office.

**Sloshing of Liquids
in Circular Canals
and Spherical Tanks**

LMSD-P LIBRARY

DDC
REF

NOV 14 1966

BORROWER'S SIGNATURE
D

LMSD LIBRARY PROPERTY
PALO ALTO

Borrower is responsible for safe keeping of this item and for
its return to LMSD Library within loan period. If this item
is not returned, borrower must provide replacement copy or
reimburse LMSD Library.

LOCKHEED AIRCRAFT CORPORATION
MISSILE SYSTEMS DIVISION
SUNNYVALE, CALIFORNIA

LMSD-5151
3 DECEMBER 1958

Stoshing of Liquids in Circular Canals and Spherical Tanks

By Bernard Budiansky

MSD-P LIBRARY

**LOCKHEED AIRCRAFT CORPORATION
MISSILE SYSTEMS DIVISION
SUNNYVALE, CALIFORNIA**

This document is subject to
special export controls and
each transmittal to foreign
nationals may be made only
with prior approval of
AFFSD CODE SS

FOREWORD

This report summarizes the results of a study undertaken by Dr. Bernard Budiansky for LMSD Research, Lockheed Aircraft Corporation. The work was performed under Air Force Contract No. AF-34(647)-181. Dr. Budiansky, consultant to Lockheed during the summer of 1958, is Associate Professor of Structural Mechanics at Harvard University.

ABSTRACT

Theoretical calculations are made of the natural modes and frequencies of small-amplitude sloshing of liquids in partially filled circular canals and spherical tanks. An integral-equation approach is used to analyze the circular canal for arbitrary depth of liquid. A similar approach for the spherical tank provides modes and frequencies for the nearly-full and half-full cases. These results, together with the known behavior of the nearly-empty tank, are used in conjunction with the trends established for the circular canal as a basis for estimating frequencies for arbitrary depth of liquid in the spherical tank. The dynamic analysis of the container-fluid system by means of the mode-superposition approach is discussed, and modal parameters required in such analyses are presented.

CONTENTS

Section		Page
	FOREWORD	ii
	ABSTRACT	iii
	LIST OF ILLUSTRATIONS	v
	NOTATION	vi
1	INTRODUCTION	1-1
2	SLOSHING MODES AND FREQUENCIES	2-1
	2.1 Basic Differential Equations	2-1
	2.2 Circular Canal	2-2
	2.3 Spherical Tank	2-13
3	SLOSHING FORCES AND MOTION	3-1
	3.1 Circular Canal	3-6
	3.2 Spherical Tank	3-7
4	NUMERICAL RESULTS	4-1
	4.1 Circular Canal	4-1
	4.2 Spherical Tank	4-6
5	COMPARISON WITH EXPERIMENT	5-1
6	CONCLUSIONS	6-1
7	REFERENCES	7-1
 Appendix		
A	NUMERICAL SOLUTION OF INTEGRAL EQUATIONS	A-1

LIST OF ILLUSTRATIONS

Figure	Page
2-1 Container Partially Filled With Liquid	2-3
2-2 Geometrical Parameters and Coordinates for Circular Canal and Spherical Tank	2-3
2-3 Nondimensional Geometrical Parameters and Coordinates for Circular Canal and Spherical Tank	2-5
2-4 Location of Source-Sink Pair in Symmetrized Domain	2-5
2-5 Conformal Mapping Sequence	2-7
2-6 Limiting Case of Nearly-Full Container	2-10
2-7 Coordinates in Free Surface of Spherical Tank	2-14
2-8 Geometrical Parameters in Equatorial Plane of Sphere	2-17
4-1 Frequencies for Circular Canal and Spherical Tank	4-2
4-2 Modal Parameters for Circular Canal	4-4
4-3 Mode Shapes for Circular Canal	4-5
4-4 Modal Parameters for Spherical Tank	4-8
4-5 Mode Shapes for Spherical Tank	4-9
5-1 Experimental Frequencies for Spherical Tank	5-1

NOTATION

x, y, z	geometrical coordinates (see Fig. 2-1)
$\xi, \bar{\xi}, \eta$	nondimensional coordinates
R	canal or sphere radius
a, e, β	geometrical parameters related to liquid depth
u, v, w	velocity distributions in x , y , and z directions, respectively
ω	oscillation frequency
t	time
ϕ, ψ, Ω	velocity potentials
Ψ	displacement potential
g	acceleration of free fall relative to container wall
λ	frequency parameter: $\lambda = \omega^2 R/g$
h	liquid depth (variable)
z, ρ	complex variables
F	complex potential
G	kernel function (circular canal)
H	kernel function (spherical tank)
w_n	mode shape for circular canal
f_n	mode shape for spherical tank
$g(\rho)$	$\sqrt{\rho} f(\rho)$
r, y, θ	cylindrical coordinate system
$\rho, \bar{\rho}$	nondimensional coordinates
m	$\rho/\bar{\rho}$
s	$\bar{\rho}\rho$
K, E	complete elliptic integrals of first and second kind, respectively

N	Neumann function for sphere
α_n, β_n	modal parameters
A_n, B_n, C_n, D_n	nondimensional modal parameters
M_c	mass of container
ρ_L	density of liquid
M_L	mass of liquid
X	external transverse force acting on container
F_S	sloshing force acting on container
U	transverse displacement of container
A	square matrix
T	integrating matrix
{}	column matrix
[]	row matrix
m,n,j,k,N	integers
Δ	interval of subdivision ($\Delta = 1/N$)

Section 1

INTRODUCTION

For sufficiently small amplitudes of motion, the dynamic effects of the sloshing of a liquid in a partially filled container can be analyzed in terms of the natural modes and frequencies of the small, free-surface oscillations of the liquid. This paper is concerned with the calculation of the modes and frequencies of partially filled circular canals and spherical tanks, with attention restricted to the modes that would be induced by lateral accelerations of the containers. The usual assumptions of inviscid, incompressible flow are made, and the container is considered to be rigid. The dynamic analysis of the container-fluid system by means of the mode-superposition approach is discussed, and modal parameters required in such analyses are presented.

The case of the half-full circular canal was considered by Rayleigh (see Ref. 1, p. 444), who carried out an approximate energy solution for the fundamental frequency. Graham (Ref. 2) estimated the fundamental frequency of the half-full sphere by conceptually dividing the liquid into a collection of half-disks and then using Rayleigh's result in an unspecified averaging process.

The frequency and mode calculations of this paper are based on a rigorous integral equation approach. In the case of the circular canal, the appropriate integral equation is formulated explicitly for an arbitrary depth of liquid, and numerical calculations of the first three pertinent modes and frequencies are performed for a range of depths by means of a matrix

approximation to the integral equation. For the spherical tank, rigorous analyses are made for only the nearly-empty, half-full, and nearly-full tanks; results for the intermediate depths are estimated by interpolation and by means of the trends established for the circular canal.

The results for the fundamental frequency for the spherical tank are compared with available experimental data.

Section 2
SLOSHING MODES AND FREQUENCIES

2.1 BASIC DIFFERENTIAL EQUATIONS

The differential equation and boundary conditions governing free-surface oscillations (Ref. 1, p. 363) will be displayed.

The liquid is supposed to be bounded by a horizontal free surface F and a rigid wetted surface S (see Fig. 2-1), and small, harmonic oscillations are assumed. The velocities in the x, y, z directions, respectively, are then

$$\begin{aligned} u & (x, y, z) \sin \omega t. \\ v & (x, y, z) \sin \omega t. \\ w & (x, y, z) \sin \omega t. \end{aligned} \quad (2.1)$$

where ω is the circular frequency.

Since the flow is irrotational, there exists a velocity potential

$$\phi (x, y, z) \sin \omega t.$$

such that

$$\begin{aligned} u & = \frac{\partial \phi}{\partial x} \\ v & = \frac{\partial \phi}{\partial y} \\ w & = \frac{\partial \phi}{\partial z} \end{aligned} \quad (2.2)$$

The continuity equation for incompressible flow is

$$\nabla^2 \phi = 0 \quad (2.3)$$

The condition of tangential flow at the rigid surface requires that

$$\nabla \phi \cdot \vec{n} \equiv \frac{\partial \phi}{\partial n} = 0 \text{ on } S \quad (2.4)$$

where \vec{n} is the unit normal vector to S .

Finally, the condition of constant pressure at the free surface together with the linearized Bernoulli equation leads to the condition

$$\frac{\partial \phi}{\partial y} = \left(\frac{\omega^2}{g} \right) \phi \text{ on } F \quad (2.5)$$

where g is the acceleration of free fall relative to the container.

Equations (2.3), (2.4), and (2.5) govern the eigenvalue problem for the frequency ω . Note that (2.1), (2.2), and (2.5) imply that the shape of the vertically displaced free surface during oscillation is given by $\phi(x, 0, z)$.

The analogous two-dimensional problem of transverse sloshing in a uniform channel is formulated in an obvious fashion by suppressing the z coordinate.

2.2 CIRCULAR CANAL

The geometrical parameters for the partially filled circular canal are shown in Fig. 2-2; the depth of liquid is measured by e , which varies from -1 for the empty canal to 1 for the full vessel.

It is clear that, because of geometrical symmetry, the natural modes involve free-surface vertical displacements that are either symmetrical or antisymmetrical about the origin. Since the symmetrical modes would not be induced by

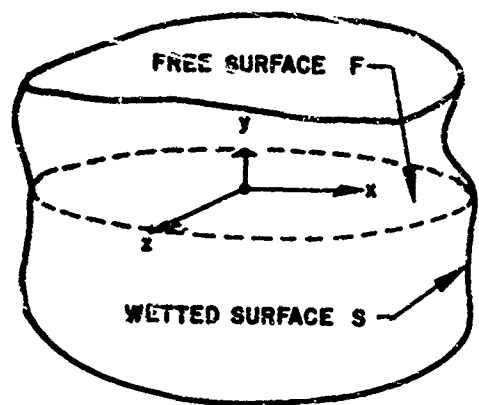


Fig. 2-1 Container Partially Filled With Liquid

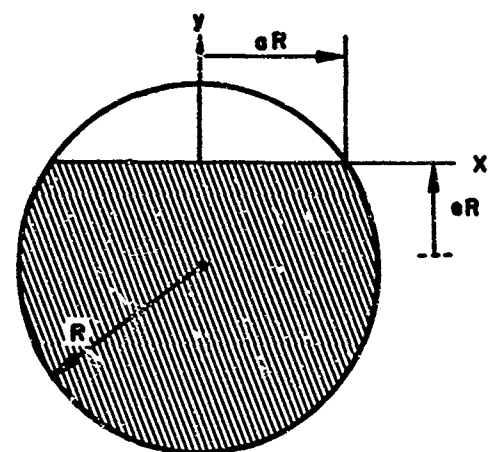


Fig. 2-2 Geometrical Parameters and Coordinates
for Circular Canal and Spherical Tank

2-3

transverse motion of the canal, attention is restricted to the antisymmetrical modes.

It is convenient to nondimensionalize the problem by introducing

$$\xi = \frac{x}{aR}$$

$$\eta = \frac{y}{aR} \quad (2.6)$$

The normalized geometry is shown in Fig. 2-3; the free-surface condition becomes

$$\frac{\partial \phi}{\partial \eta} = (\lambda a) \phi \quad (2.7)$$

where $\lambda = \frac{\omega^2 R}{g}$. The angle β shown in Fig. 2-3 is given by

$$\beta = \arcsin e \quad (2.8)$$

and varies from $\pi/2$ for the full canal to $-\pi/2$ for the empty canal.

The procedure for setting up an integral equation governing the antisymmetrical modes follows.

Consider the fluid-filled container consisting of the original wetted boundary plus its reflection about the ξ axis (Fig. 2-4). Place a two-dimensional sink of strength $2w(\xi)d\xi$ at ξ and a source of equal strength at $-\xi$, and smear out both over a strip of length $d\xi$. Denote the resulting velocity potential for the internal flow by

$$v(\xi) \Phi(\xi, \eta; \bar{\xi}) d\xi$$

Since the velocity potential is arbitrary to within a constant, it will be assumed that $\Phi(0, \eta; \bar{\xi}) = 0$, and hence $\Phi(\xi, \eta; \bar{\xi}) = -\Phi(-\xi, \eta; \bar{\xi})$. By

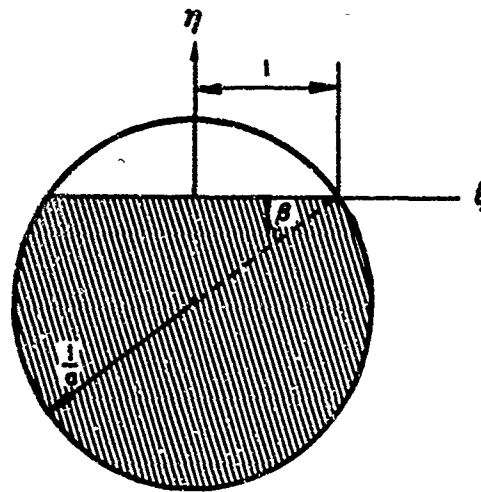


Fig. 2-3 Nondimensional Geometrical Parameters
and Coordinates for Circular Canal
and Spherical Tank

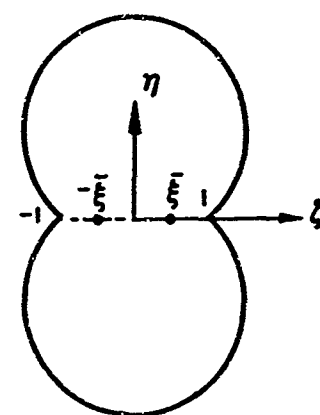


Fig. 2-4 Location of Source-Sink Pair in
Symmetrized Domain

symmetry, the vertical velocities along $\eta = 0$ vanish everywhere except on the strips of length $d\xi$ at ξ and $-\xi$, where just below the ξ axis they are $w(\xi)$ and $-w(\xi)$, respectively. It is now possible to construct the velocity potential for the free-surface oscillation of the configuration of Fig. 2-3 by means of a distribution of sources and sinks along the ξ axis. It is necessary only to satisfy the free-surface condition [Eq. (2.7)] relating the vertical velocities along the ξ axis to the velocity potential along the ξ axis. Thus, we require that

$$w(\xi) = (\lambda a) \int_0^1 \Phi(\xi, 0; \bar{\xi}) w(\bar{\xi}) d\bar{\xi} \quad (2.9)$$

for $0 \leq \xi \leq 1$; since $\Phi(-\xi, 0; \bar{\xi}) = -\Phi(\xi, 0; \bar{\xi})$, Eq. (2.9) is automatically satisfied for negative ξ , with $w(-\xi) = -w(\xi)$.

The problem now is to find the kernel function

$$G(\xi, \bar{\xi}) \equiv \Phi(\xi, 0; \bar{\xi}) \quad (2.10)$$

and this is readily accomplished by conformal mapping.

The successive transformations shown in Fig. 2-5 map the region of Fig. 2-4 into the entire f plane; the resultant transformation is

$$f = \left[\frac{1}{2} \left(\frac{1-z}{1+z} \right) \right]^\gamma \quad (2.11)$$

where $\gamma = \frac{2}{1+2\beta/\pi}$. Now let f_1 and f_2 correspond to $z = \bar{\xi}$ and $-\bar{\xi}$, respectively. The complex potential of a sink at f_1 and a source at f_2 , each of strength 2, is

$$F = -\frac{1}{\pi} \log \left(\frac{f-f_1}{f-f_2} \right) + g(\bar{\xi}) \quad (2.12)$$

where g is an arbitrary function of $\bar{\xi}$.

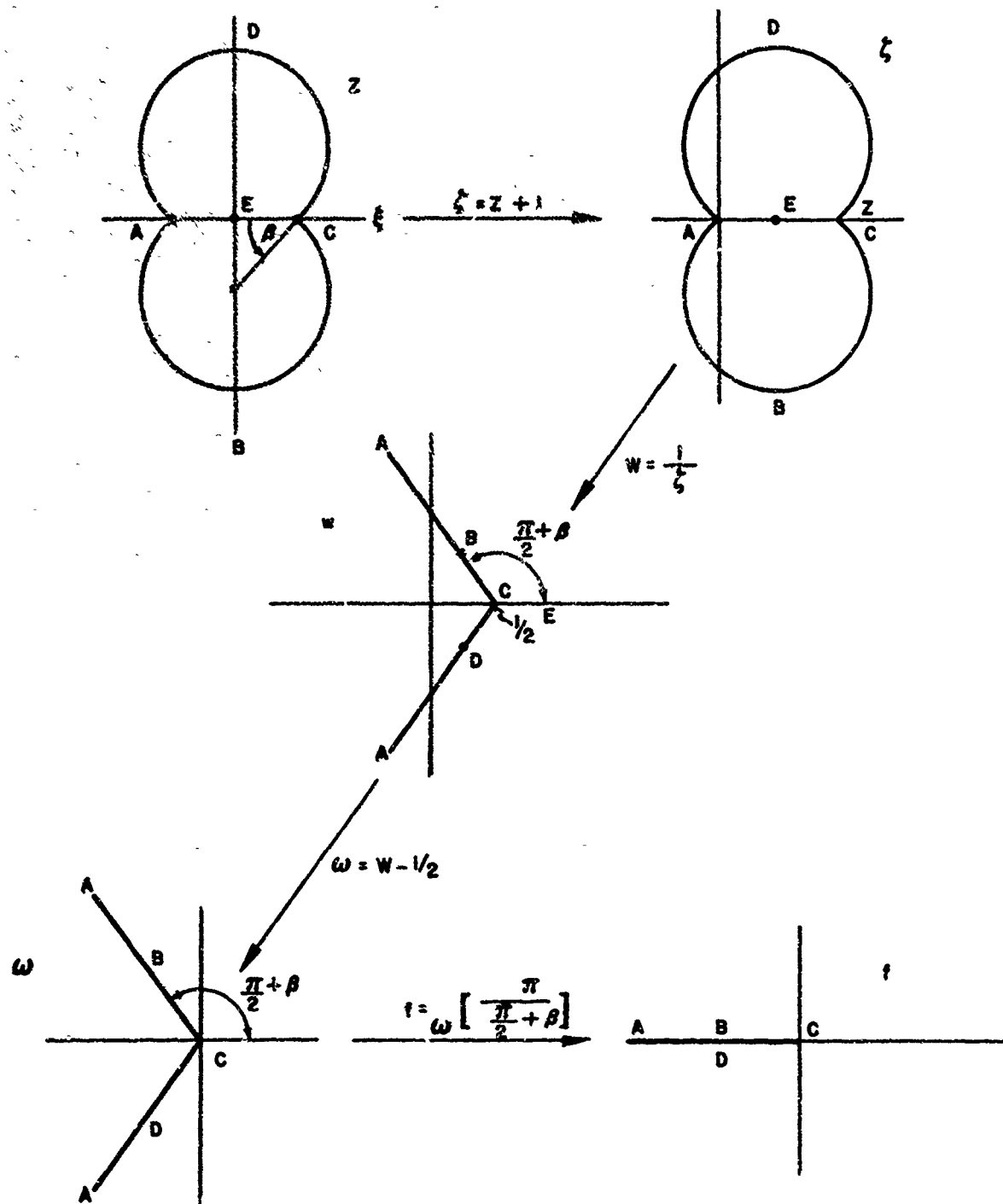


Fig. 2-5 Conformal Mapping Sequence

2-7

Substituting Eq. (2.11) into Eq. (2.12) gives, in the z plane, the corresponding potential

$$F = -\frac{1}{\pi} \log \left[\frac{\left(\frac{1-z}{1+z}\right)^{\gamma} - \left(\frac{1-\bar{\xi}}{1+\bar{\xi}}\right)^{\gamma}}{\left(\frac{1-z}{1+z}\right)^{\gamma} + \left(\frac{1-\bar{\xi}}{1+\bar{\xi}}\right)^{\gamma}} \right] + g(\bar{\xi})$$

Now choose g so that $F(0) = 0$; then

$$\begin{aligned} F(z) &= -\frac{1}{\pi} \log \left\{ \frac{\left(\frac{1-z}{1+z}\right)^{\gamma} - \left(\frac{1-\bar{\xi}}{1+\bar{\xi}}\right)^{\gamma}}{\left(\frac{1-z}{1+z}\right)^{\gamma} + \left(\frac{1-\bar{\xi}}{1+\bar{\xi}}\right)^{\gamma}} \right\} \left[\frac{1 - \left(\frac{1+\bar{\xi}}{1-\bar{\xi}}\right)^{\gamma}}{1 - \left(\frac{1-\bar{\xi}}{1+\bar{\xi}}\right)^{\gamma}} \right] \\ &= -\frac{1}{\pi} \log \left\{ \frac{(1-z)^{\gamma} (1+\bar{\xi})^{\gamma} - (1-z)^{\gamma} (1-\bar{\xi})^{\gamma}}{(1+z)^{\gamma} (1+\bar{\xi})^{\gamma} - (1-z)^{\gamma} (1-\bar{\xi})^{\gamma}} \right\} \end{aligned}$$

Finally, $G(\xi, \bar{\xi}) = \operatorname{Re} F(z)$ is

$$G(\xi, \bar{\xi}) = -\frac{1}{\pi} \log \left| \frac{(1+\xi)^{\gamma} (1-\bar{\xi})^{\gamma} - (1-\xi)^{\gamma} (1+\bar{\xi})^{\gamma}}{(1+\xi)^{\gamma} (1+\bar{\xi})^{\gamma} - (1-\xi)^{\gamma} (1-\bar{\xi})^{\gamma}} \right| \quad (2.13)$$

Note that G has a logarithmic singularity at $\xi = \bar{\xi}$. Note also that

$$G(\xi, \bar{\xi}) = G(\bar{\xi}, \xi) = -G(-\xi, \bar{\xi})$$

To recapitulate, then, the solutions of the homogeneous (singular) integral equation

$$w(\xi) = (\lambda a) \int_0^1 G(\xi, \bar{\xi}) w(\bar{\xi}) d\bar{\xi} \quad (2.14)$$

with $G(\xi, \bar{\xi})$ given by Eq. (2.13), provide the characteristic free-surface shapes $w(\xi)$, and the associated eigenvalues of (λa) yield the natural frequencies.

The numerical solution of the integral equation (2.14) has been performed for various depths on the basis of the matrix formulation described in Appendix A. The results are presented in Section 4.

Special cases. Several special cases for which approximate solutions can easily be obtained are of particular interest. For the half-full canal ($e = 0$), the kernel becomes

$$G(\xi, \bar{\xi}) = -\frac{1}{\pi} \log \left| \frac{(\xi - \bar{\xi})(1 - \xi\bar{\xi})}{(\xi + \bar{\xi})(1 + \xi\bar{\xi})} \right|$$

A one-term Galerkin-type solution for the lowest frequency can be carried out without difficulty for this case.

From Eq. (2.14),

$$\int_0^1 [w(\xi)]^2 d\xi = (\lambda a) \int_0^1 \int_0^1 G(\xi, \bar{\xi}) w(\bar{\xi}) w(\xi) d\xi d\bar{\xi} \quad (2.15)$$

Introducing the approximate mode shape $w = \xi$ into Eq. (2.15) and carrying out the integrations give, for $e = 0$, ($a = 1$), the approximate fundamental eigenvalue

$$\lambda_1 \approx \frac{1}{3 \left[\frac{2}{\pi} - \frac{\pi}{8} \right]} = 1.367 \quad (2.16)$$

or

$$\omega_1 \approx 1.169 \left(\frac{g}{R} \right)^{1/2}$$

This is precisely the result found by Rayleigh in an entirely different way. The result is necessarily an upper bound to the exact frequency. Rayleigh also obtained an improved approximation $\omega \approx 1.1644 \left(\frac{g}{R} \right)^{1/2}$.

Also of special interest is the limiting case of the nearly-full canal, where $\beta \rightarrow \frac{\pi}{2}$ and $\gamma \rightarrow 1$. The integral equation becomes simply

$$w(\xi) = -(\lambda a) \int_0^1 \frac{1}{\pi} \log \left| \frac{\xi - \bar{\xi}}{\xi + \bar{\xi}} \right| w(\bar{\xi}) d\bar{\xi} \quad (2.17)$$

Denote the critical values of (λa) by c_n ($n = 1, 2, \dots$); then, for e sufficiently close to 1,

$$\begin{aligned} \lambda_n &\approx \frac{c_n}{a} \\ &= \frac{c_n}{\sqrt{1 - e^2}} \end{aligned}$$

Thus, the frequencies tend to infinity as the full condition is approached. This result, as well as the form of the integral equation (2.17), could have been anticipated by consideration of the sloshing of liquid in a half plane with a rigid boundary having an aperture of length $(2aR)$. (See Fig. 2-6.) The kernel function for this case can be written directly in terms of a source-sink pair, without the need for conformal transformations. A one-term Galerkin solution of Eq. (2.17), again with $w = \xi$, gives the approximate result

$$c_1 \approx 2\pi/3 = 2.094 \quad (2.18)$$

so that

$$\lambda_1 \approx \frac{2.094}{\sqrt{1 - e^2}}$$

for

$$e \rightarrow 1.$$

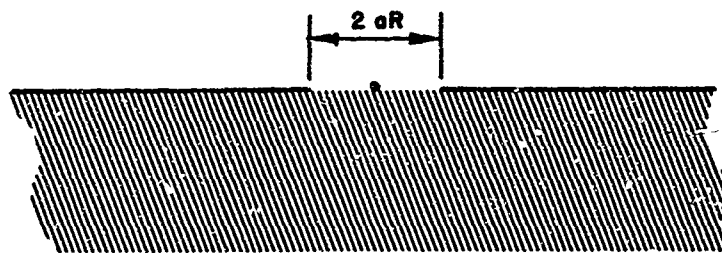


Fig. 2-6 Limiting Case of Nearly-Full Container

For the nearly-empty canal ($e \rightarrow -1$), γ becomes infinite. The asymptotic results for this case are most readily found by abandoning the integral equation and exploiting shallow-water theory. (See Ref. 1, p. 291.) The differential equation for the velocity potential may be conveniently deduced from the variational principle given by Lawrence, Wang, and Reddy (Ref. 3). The variational equation is

$$\delta \left[\int_V \left| \nabla \phi \right|^2 dV - \frac{\omega^2}{2g} \int_F \phi^2 dF \right] = 0 \quad (2.19)$$

where V denotes the volume of fluid in Fig. 2-1.

As shown in Ref. 3, Eqs. (2.3), (2.4), and (2.5) constitute the Euler equation and natural boundary conditions of Eq. 2.19.

For the two-dimensional canal of shallow depth variation $h(x)$, it is assumed that ϕ may be taken independent of y . Then Eq.(2.19) becomes

$$\delta \left[\frac{1}{2} \int_F h(x) \left[\frac{d\phi}{dx} \right]^2 dx - \frac{\omega^2}{2g} \int_F \phi^2 dx \right] = 0$$

The Euler equation is

$$\frac{d}{dx} \left[h \frac{d\phi}{dx} \right] + \frac{\omega^2}{g} \phi = 0 \quad (2.20)$$

For the nearly empty circular canal, the depth has approximately the parabolic variation

$$h(x) = \frac{1}{2R} \left[(aR)^2 - x^2 \right]$$

so that Eq.(2.20) becomes

$$\frac{1}{2} \frac{d}{dx} \left[(aR)^2 - x^2 \frac{d\phi}{dx} \right] + \left(\frac{\omega^2 R}{g} \right) \phi = 0$$

or, in terms of $\xi = \frac{x}{aR}$,

$$\frac{1}{2} \frac{d}{d\xi} \left[(\xi^2 - 1) \frac{d\phi}{d\xi} \right] - \lambda \phi = 0$$

whence

$$(\xi^2 - 1) \phi'' + 2\xi \phi' - 2\lambda \phi = 0 \quad (2.21)$$

This is essentially Legendre's differential equation. For the antisymmetrical modes, $\phi(0) = 0$; in addition, the condition of finiteness at $\xi = 1$ is imposed. The solutions of Eq. (2.21) are then the odd-order Legendre polynomials of the first kind

$$P_{2n-1}(\xi) \quad n = 1, 2, 3, \dots \quad (2.22)$$

with the corresponding eigenvalues

$$\lambda_n = 2n^2 - n \quad n = 1, 2, 3, \dots \quad (2.23)$$

The polynomials (Eq. [2.22]) represent the limiting free-surface shapes of the natural modes as the depth approaches zero.

The first eigenvalue is $\lambda_1 = 1$, and so the fundamental frequency

$$\omega_1 = \sqrt{\frac{g}{R}}$$

is, as could be expected, simply the frequency of a pendulum of length R .

2.3 SPHERICAL TANK

The geometrical parameters of Figs. 2-2 and 2-3 may be considered to apply to the spherical tank. A rigorous analysis was executed for only the nearly-full and half-full cases; rigorous results for the nearly empty case, given by Lamb (Ref. 1, p. 291), are also available.

Introduce the cylindrical coordinate system (r, y, θ), where $x = r \cos \theta$, $z = r \sin \theta$. The appropriate nondimensional system becomes (ρ, η, θ) , where $\rho = r/aR$, and, as before, $\eta = y/aR$. In these nondimensional coordinates, the governing differential equation is:

$$\frac{\partial^2 \phi}{\partial \rho^2} + \frac{1}{\rho} \frac{\partial \phi}{\partial \rho} + \frac{\partial^2 \phi}{\partial \eta^2} + \frac{1}{\rho^2} \frac{\partial^2 \phi}{\partial \theta^2} = 0 \quad (2.24)$$

and the free-surface boundary condition remains that given in Eq. (2.7). It is evident that solutions for the modes may be written in the form

$$\phi = \psi(\rho, \eta) \cos k\theta \quad (k = 1, 2, \dots) \quad (2.25)$$

It will be shown later that only the modes with $k = 1$ are induced by lateral accelerations in the ξ direction. Consequently, attention will be restricted to these cases.

The procedure for setting up an integral equation analogous to Eq. (2.14) is as follows. Consider the volume of fluid enclosed by the wetted surface and its reflection about the originally free surface $\eta = 0$. (See Fig. 2-4.) Now, in the plane $\eta = 0$ (Fig. 2-7), place a distribution of three-dimensional sinks along the annulus $(\bar{\rho}, \bar{\rho} + d\bar{\rho})$ of strengths $2f(\bar{\rho}) \cos \alpha$ per unit area. Let $f(\bar{\rho}) \Omega(\rho, \eta, \theta; \bar{\rho}) \bar{\rho} d\bar{\rho}$ be the resulting velocity potential. Then, since the vertical velocity just below the plane $\eta = 0$ is, because of this potential, zero everywhere except in the annulus, where it is

$f(\bar{\rho}) \cos \theta$, the imposition of the boundary condition Eq. (2.7) at $\theta = 0$ requires that

$$f(\rho) = (\lambda a) \int_0^1 \Omega(\rho, 0, 0; \bar{\rho}) \bar{\rho} f(\bar{\rho}) d\bar{\rho} \quad (2.26)$$

It is convenient to let $g(\rho) = \sqrt{\rho} f(\rho)$; then

$$g(\rho) = (\lambda a) \int_0^1 H(\rho, \bar{\rho}) g(\bar{\rho}) d\bar{\rho} \quad (2.27)$$

where

$$H(\rho, \bar{\rho}) = \sqrt{\rho \bar{\rho}} \Omega(0, 0, 0; \bar{\rho}) \quad (2.28)$$

The problem now is to determine $H(\rho, \bar{\rho})$.

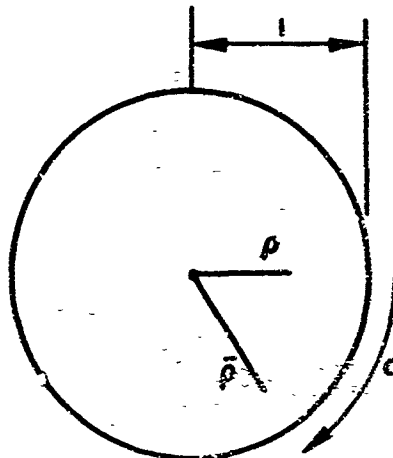


Fig. 2-7 Coordinates in Free Surface of Spherical Tank

2.3.1 Nearly-Full Tank

For the nearly-full case, the symmetrized region is the entire space (Fig. 2-6), and the potential of a sink in the plane $\eta = 0$ is unmodified by the presence of a rigid boundary in this plane. The potential of a sink of strength 2 at $(\bar{\rho}, 0, \alpha)$ is

$$\frac{1}{2\pi} \left[(\rho \cos \theta - \bar{\rho} \cos \alpha)^2 + (\rho \sin \theta - \bar{\rho} \sin \alpha)^2 + \eta^2 \right]^{1/2}$$

and so

$$\Omega(\rho, 0, 0; \bar{\rho}) = \frac{1}{2\pi} \int_0^{2\pi} \frac{\cos \alpha d\alpha}{\left[\rho^2 + \bar{\rho}^2 - 2\rho\bar{\rho} \cos \alpha \right]^{1/2}}$$

Then,

$$\tilde{\Omega}(\rho, \bar{\rho}) = \left(\frac{1}{\pi} \right) \sqrt{\rho\bar{\rho}} \int_0^\pi \frac{\cos \alpha d\alpha}{\left[\frac{\rho^2}{\bar{\rho}^2} + \bar{\rho}^2 - 2\rho\bar{\rho} \cos \alpha \right]^{1/2}}$$

Clearly, $H(\rho, \bar{\rho}) = H(\bar{\rho}, \rho)$. Consider $\rho < \bar{\rho}$, and let $m = \left(\frac{\rho}{\bar{\rho}} \right)$. Then,

$$H = \frac{\sqrt{m}}{\pi} \int_0^\pi \frac{\cos \alpha d\alpha}{\left[m^2 - 2m \cos \alpha + 1 \right]^{1/2}} \quad (2.29)$$

Letting $\beta = \frac{\alpha}{2}$ yields

$$H = \frac{q}{\pi} \int_0^{\pi/2} \frac{(2 \sin^2 \beta - 1) d\beta}{\left[1 - q^2 \sin^2 \beta \right]^{1/2}} \quad (2.30)$$

$$\text{where } q = \frac{2\sqrt{m}}{m+1}$$

This may be evaluated in terms of complete elliptic integrals (Ref. 4, p. 73) to give

$$H = \frac{1}{\pi} \left[\left(\frac{2}{q} - q \right) K(q) - \frac{2}{q} E(q) \right] \quad (2.31)$$

where

$$K(q) = \int_0^{\frac{\pi}{2}} \left[1 - q^2 \sin^2 \theta \right]^{1/2} d\theta$$

and

$$E(q) = \int_0^{\frac{\pi}{2}} \left[1 - q^2 \sin^2 \theta \right]^2 d\theta$$

are the complete elliptic integrals of the first and second kind, respectively.

The result (Eq.[2.31]) for $H(\rho, \bar{\rho})$ may be put into a much more convenient form by exploiting the Landen transformations (Ref. 5)

$$K(m) = \left(\frac{1}{1+m} \right) K(q)$$

$$E(m) = \left(\frac{1+m}{2} \right) E(q) + \left(\frac{1-m}{2} \right) K(q)$$

to give, as a final result

$$H(\rho, \bar{\rho}) = \frac{2}{\sqrt{\frac{\rho}{\bar{\rho}}}} \left[K\left(\frac{\rho}{\bar{\rho}}\right) - E\left(\frac{\rho}{\bar{\rho}}\right) \right] \quad (2.32)$$

for $\rho < \bar{\rho}$. Since $H(\rho, \bar{\rho}) = H(\bar{\rho}, \rho)$, the kernel is completely defined. This kernel, like the ones for the circular canal, also has a logarithmic singularity at $\rho = \bar{\rho}$.

2.3.2 Half-Full Tank

For the half-full case, the symmetrized volume is a complete sphere, and so the kernel function can be evaluated on the basis of the known Neumann function (or Dirichlet function of the second kind) for the sphere. Thus (see Ref. 6) the function of the position Q (Fig. 2-8) given by

$$N(Q) = \frac{1}{2\pi} \left\{ \frac{1}{\bar{P}Q} + \frac{1}{(\bar{O}P)(\bar{Q}P')} + \log \frac{2}{1 - (\bar{O}Q)(\bar{O}P) \cos \gamma + (\bar{O}P)(\bar{Q}P')} \right\} \quad (2.33)$$

satisfies the following conditions in the unit sphere:

- (1) $N(Q)$ is harmonic.
- (2) $N(Q)$ has a sink of strength 2 at P .
- (3) The normal derivative of $N(Q)$ has the constant value $-\left(\frac{1}{2\pi}\right)$ at the surface of the sphere.

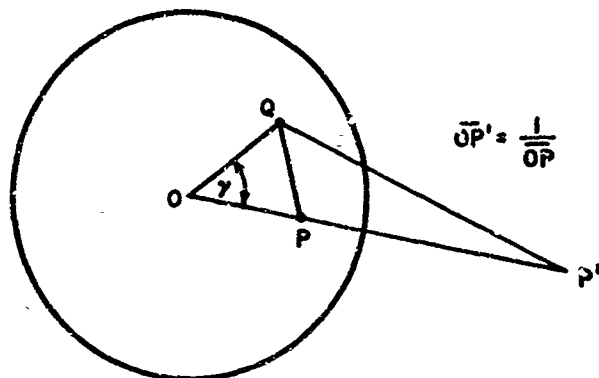


Fig. 2-8 Geometrical Parameters in Equatorial Plane of Sphere

Now let P be the point $(\rho, 0, 0)$ in the equatorial plane of the sphere (Fig. 2-7), and let Q be the point $(\bar{\rho}, 0, \alpha)$. Then

$$N(\rho, 0, 0) = \frac{1}{2\pi} \left\{ \frac{1}{\rho^2 + \bar{\rho}^2 - 2\rho\bar{\rho} \cos \alpha}^{1/2} + \frac{1}{(\rho\bar{\rho})^2 + 1 - 2\rho\bar{\rho} \cos \alpha}^{1/2} \right. \\ \left. + \log \frac{2}{1 - \rho\bar{\rho} \cos \alpha + (\rho\bar{\rho})^2 + 1 - 2\rho\bar{\rho} \cos \alpha}^{1/2} \right\}$$

and therefore

$$H(\rho, \bar{\rho}) = \frac{\sqrt{\rho\bar{\rho}}}{\pi} \int_0^\pi \frac{\cos \alpha d\alpha}{\rho^2 + \bar{\rho}^2 - 2\rho\bar{\rho} \cos \alpha}^{1/2} + \frac{\sqrt{\rho\bar{\rho}}}{\pi} \int_0^\pi \frac{\cos \alpha d\alpha}{(\rho\bar{\rho})^2 + 1 - 2\rho\bar{\rho} \cos \alpha}^{1/2} \\ + \frac{\sqrt{\rho\bar{\rho}}}{\pi} \int_0^\pi \cos \alpha \left[\log \frac{2}{1 - \rho\bar{\rho} \cos \alpha + (\rho\bar{\rho})^2 + 1 - 2\rho\bar{\rho} \cos \alpha}^{1/2} \right] d\alpha \quad (2.34)$$

Note that, because of the cosine variation of local sink strength at the radius $\bar{\rho}$, the normal flow at the spherical surface vanishes, as it should, despite the fact that the Neumann function (Eq. [2.33]) for a single sink produces a constant flux at the surface.

The evaluation of the first two integrals in Eq. (2.34) follows immediately from the results for the nearly-full case; the last integral may be evaluated as follows. Let $s = (\rho\rho)$, and let

$$\begin{aligned} I(s) &= \int_0^\pi \cos \alpha \log \left\{ \frac{2}{\{1 - s \cos \alpha + (s^2 + 1 - 2s \cos \alpha)\}^{1/2}} \right\} d\alpha \\ &= - \int_0^\pi \cos \alpha \log \left[(1 - s \cos \alpha) + (s^2 + 1 - 2s \cos \alpha)^{1/2} \right] d\alpha \end{aligned} \quad (2.55)$$

Note that $I(0) = 0$; subtract the zero quantity $\int_0^\pi (\cos \alpha) \log s d\alpha$ from Eq. (2.55), giving

$$I(s) = - \int_0^\pi \cos \alpha \log \left\{ \frac{1}{s} - \cos \alpha + \left[1 + \frac{1}{s^2} - \frac{2 \cos \alpha}{s} \right]^{1/2} \right\} d\alpha$$

Then, by differentiation under the integral sign, it is found that

$$I'(s) = \frac{1}{s} \int_0^\pi \frac{\cos \alpha d\alpha}{[s^2 + 1 - 2s \cos \alpha]^{1/2}}$$

which (see Eqs. [2.29] and [2.32]) is

$$\frac{2}{s^2} \left[K(s) - E(s) \right]$$

Hence

$$I(s) = \int_0^s \frac{2}{s^2} \left[K(s) - E(s) \right] ds$$

which gives (Ref. 7, p. 273)

$$I(s) = \frac{2}{s} \left[E(s) - (1 - s^2) K(s) \right]$$

Then, with $m = \frac{\rho}{\bar{\rho}}$ ($\rho < \bar{\rho}$), evaluation of the three integrals in Eq. (2.34) gives:

$$\begin{aligned} H(\rho, \bar{\rho}) &= \frac{1}{\pi} \left\{ \frac{2}{\sqrt{m}} \left[K(m) - E(m) \right] + \frac{2}{\sqrt{s}} \left[K(s) - E(s) \right] \right. \\ &\quad \left. + \frac{2}{\sqrt{s}} \left[E(s) - (1 - s^2) K(s) \right] \right\} \end{aligned}$$

or, finally,

$$H(\rho, \bar{\rho}) = \frac{1}{\pi} \left\{ \frac{2}{\sqrt{\frac{\rho}{\bar{\rho}}}} \left[K\left(\frac{\rho}{\bar{\rho}}\right) - E\left(\frac{\rho}{\bar{\rho}}\right) \right] + 2 \left(\frac{\rho}{\bar{\rho}} \right)^{3/2} K\left(\frac{\rho}{\bar{\rho}}\right) \right\} \quad (2.36)$$

for $\rho < \bar{\rho}$. Again, the additional fact that $H(\rho, \bar{\rho}) = H(\bar{\rho}, \rho)$ (see Eq. [2.34]) completely defines $H(\rho, \bar{\rho})$.

As in the case of the circular canal, the solutions of the integral equation (2.27), with the kernels Eq. 2.32 and 2.36, were performed on the basis of the matrix set-up discussed in Appendix A. The results are given in Section 4.

2.3.3 Nearly-Empty Tank

The nearly-empty tank may be analyzed in a fashion analogous to the treatment of the nearly-empty circular canal by approximating the wetted surface with the paraboloid of revolution having the depth variation

$$h(r) = \frac{1}{2R} \left[(z_1)^2 - r^2 \right]$$

and using shallow-water theory. The problem of oscillation in such a container has been solved by Lamb (Ref. 1, p. 291); the pertinent parts of the solution are repeated here in a convenient form. By assuming $\phi = f(\rho) \cos \theta$ (independent of η), the governing differential equation for f can be found from the variational principle (Eq. [2.19]) to be

$$\rho^2(\rho^2 - 1) f'' + \rho(3\rho^2 - 1) f' + \left[1 - (2\lambda + 1) \rho^2 \right] f = 0 \quad (2.37)$$

or

$$\left[\rho(\rho^2 - 1) f \right]' + \left[\frac{1}{\rho} - (2\lambda + 1)\rho \right] f = 0 \quad (2.38)$$

Then, appropriate boundary conditions are that $f = 0$ at $\rho = 0$, and f is finite at $\rho = 1$. Note, then, for future use, that Eq. (2.38) implies that the orthogonality condition

$$\int_0^1 \rho f_m(\rho) f_n(\rho) = 0 \quad (2.39)$$

holds for eigenfunctions f_m and f_n associated with distinct eigenvalues λ_m and λ_n .

The solution of Eq. (2.38) for the antisymmetrical modes is

$$f_n = \sum_{j=1}^n a_j \rho^{2j-1} \quad n = 1, 2, \dots \quad (2.40)$$

where

$$a_1 = 1$$

$$a_{j+1} = - \left[\frac{n^2 - j^2}{j(j+1)} \right] a_j$$

and the corresponding eigenvalues are

$$\lambda_n = 2n^2 - 1 \quad n = 1, 2, \dots \quad (2.41)$$

The first three eigenfunctions, normalized to give $f_n(1) = 1$, are:

$$\begin{aligned} f_1 &= \rho \\ f_2 &= 5\rho^3 - 2\rho \\ f_3 &= 10\rho^5 - 12\rho^3 + 3\rho \end{aligned} \quad (2.42)$$

As in the case of the circular canal, the lowest eigenvalue is $\lambda_1 = 1$, corresponding to the frequency of a pendulum of length R . It is interesting to compare the eigenvalues for the nearly empty canal and spherical tank; from Eqs. (2.41) and (2.23):

$$(\lambda_n)_{\text{sphere}} = (\lambda_n)_{\text{canal}} + (n - 1)$$

Section 3
SLOSHING FORCES AND MOTION

Suppose that the rigid container shown in Fig. 2-1 is subjected to a displacement $U(t)$ in the x direction; tank displacements in the y and z direction, as well as rotations of the tank about all axes, are assumed to be fully constrained. Define a displacement potential Ψ for the resulting fluid displacement relative to the tank, such that the relative displacements are given by

$$\left[\frac{\partial \Psi}{\partial x}, \frac{\partial \Psi}{\partial y}, \frac{\partial \Psi}{\partial z} \right]$$

and assume Ψ in the form

$$\Psi = \sum a_n(t) \phi_n(x, y, z)$$

where the ϕ_n 's are the potentials associated with the natural modes of liquid oscillation in a stationary, rigid tank. Lagrange's equations will be the basis for establishing differential equations relating the generalized coordinates $U(t)$ and $a_n(t)$ to the external force X on the tank. The results will be used to calculate the "sloshing" forces of the liquid on the container wall.

The potential energy during motion is

$$\begin{aligned} \text{P.E.} &= \frac{1}{2} \int_F \rho_L g \left[\frac{\partial \psi}{\partial y} \right]^2 dF \\ &= \frac{1}{2} \int_F \rho_L g \left(\sum_n a_n \frac{\partial \phi_n}{\partial y} \right)^2 dF \end{aligned}$$

where ρ_L is the density.

But (see Eq.[2.5])

$$\frac{\partial \phi_n}{\partial y} = -\frac{\omega_n^2}{g} \phi_n$$

so that

$$\text{P.E.} = \frac{1}{2} \int_F \rho_L g \left(\sum_n \frac{a_n \omega_n^2}{g} \phi_n \right)^2 dF \quad (3.1)$$

Note, however, that if ϕ_m and ϕ_n are nodes corresponding to the distinct frequencies ω_m and ω_n ,

$$\begin{aligned} \int_V \nabla \phi_m \cdot \nabla \phi_n dV &= \int_V \phi_m \nabla^2 \phi_n dV - \int_S \phi_m \vec{n} \phi_n \cdot \vec{n} dS \\ &\quad - \int_F \phi_m \frac{\partial \phi_n}{\partial y} dF \end{aligned} \quad (3.2)$$

Also, by Eqs. (2.3) and (2.4), the first two integrals on the right-hand side vanish, and so, by Eq. (2.5), the right-hand side becomes

$$-\int_{\mathcal{F}} \frac{\omega_n^2}{g} \phi_m \phi_n dF \quad (3.3)$$

But then the left-hand side of Eq. (3.2) is also given by

$$-\int_{\mathcal{F}} \frac{\omega_m^2}{g} \phi_m \phi_n dF \quad (3.4)$$

and so, for $\omega_m \neq \omega_n$, the equality of Eqs. (3.3) and (3.4) implies that

$$\int_{\mathcal{F}} \phi_m \phi_n dF = 0 \quad (3.5)$$

and also

$$\int_V \nabla \phi_m \cdot \nabla \phi_n dV = 0 \quad (3.6)$$

Hence, the potential energy (Eq. [2.42]) becomes

$$P.E. = \frac{\rho_L}{2g} \int_{\mathcal{F}} \sum_n a_n^2 \omega_n^4 \phi_n^2 dF$$

or, letting $\alpha_n = \int_F \phi_n^2 dF$,

$$\text{I.E.} = \frac{\rho_L}{2g} \sum \alpha_n a_n^2 v_n^4 \quad (3.7)$$

The kinetic energy of the container-liquid system is

$$\begin{aligned} \text{K.E.} = & \frac{1}{2} M_c (\dot{U})^2 + \frac{\rho_L}{2} \int_V \left[\dot{U} + \sum \dot{a}_n \frac{\partial \phi_n}{\partial x} \right]^2 + \left[\sum \dot{a}_n \frac{\partial \phi_n}{\partial y} \right]^2 \\ & + \left[\sum \dot{a}_n \frac{\partial \phi_n}{\partial z} \right]^2 \Big| dV \end{aligned}$$

where M_c is the container mass.

Using Eqs. (3.4) and (3.5), together with the energy relation for a single mode (see Eq. [2.19])

$$\int_V \left| \nabla \phi_n \right|^2 dV = \frac{\omega_n^2}{2g} \int_F \phi_n^2 dF$$

gives

$$\text{K.E.} = \frac{1}{2} (M_c + M_L) (\dot{U})^2 + \frac{\rho_L}{2g} \sum \alpha_n \omega_n^2 (\dot{a}_n)^2 + \rho_L \sum \beta_n a_n \quad (3.8)$$

where

$$\beta_n = \int_V \frac{\partial \phi_n}{\partial x} dV \quad (3.9)$$

and M_L is the total mass of liquid.

The expression for β_n may be transformed as follows:

$$\begin{aligned} \beta_n &= \int_V \left\{ \frac{\partial}{\partial x} \left(x \frac{\partial \phi_n}{\partial x} \right) + \frac{\partial}{\partial y} \left(x \frac{\partial \phi_n}{\partial y} \right) + \frac{\partial}{\partial z} \left(x \frac{\partial \phi_n}{\partial z} \right) \right\} dV - \int_V x \nabla^2 \phi_n dV \\ &= \int_F x \frac{\partial \phi_n}{\partial y} dF + \int_S x \nabla \phi_n \cdot \vec{n} dS \end{aligned}$$

Finally,

$$\beta_n = \frac{\omega_n^2}{g} \int_F x \dot{a}_n dF \quad (3.10)$$

With the Lagrangian $L = (K.E. - P.E.)$ determined by Eqs. (3.6) and (3.7),
Lagrange's equations

$$\frac{d}{dt} \frac{\partial L}{\partial \dot{U}} - \frac{\partial L}{\partial U} = X$$

$$\frac{d}{dt} \frac{\partial L}{\partial \dot{a}_n} - \frac{\partial L}{\partial a_n} = 0$$

yield the differential equations

$$\ddot{a}_n + w_n^2 a_n = - \left(\frac{g}{\alpha_n^2} \right) \left(\frac{\beta_n}{\alpha_n} \right) \ddot{U} \quad (3.11)$$

$$(M_c + M_L) \ddot{U} + \rho_L \sum \beta_n \ddot{a}_n = X \quad (3.12)$$

The sloshing force F_S of the liquid acting on the container in the positive x direction is

$$F_S = M_c \ddot{U} - X$$

Therefore, from Eq. (3.12),

$$F_S = -M_L \ddot{U} - \rho_L \sum \beta_n \ddot{a}_n \quad (3.13)$$

These results will be cast in convenient forms for the circular canal and the spherical tank.

3.1 CIRCULAR CANAL

The quantities α_n and β_n in Eqs. (3.11)-(3.13) involve only the values of ϕ_n at the surface, which are proportional to the eigenfunctions w_n of the integral equation (2.14). For convenience, choose $w_n(1) = 1$; then

$$\beta_n = \left(\frac{2\omega_n^2}{g} \right) (aR)^2 \int_0^1 \xi w(\xi) d\xi$$

$$\alpha_n = 2(aR) \int_0^1 [w(\xi)]^2 d\xi$$

Introduce, now, the slosh height ξ_n at the right-hand side of the canal associated with the n^{th} mode:

$$\xi_n = a_n \frac{\partial \phi}{\partial y} (aR)$$

$$= (a_n) \frac{\omega_n^2}{g} w_n(1)$$

$$= \frac{a_n \omega_n^2}{g}$$

The total height of slosh at the wall is then $\sum \xi_n$. Equations (3.10)-(3.12) may then be modified to:

$$\ddot{\xi}_n + \omega_n^2 \xi_n = - (\lambda_n A) \frac{B_n}{A_n} \ddot{U} \quad (3.14)$$

$$(M_C + M_L) \ddot{U} + 2\omega_L (aR)^2 \sum B_n \ddot{\xi}_n = X \quad (3.15)$$

$$F_S = -M_L \ddot{U} - 2\rho_L (aR)^2 \sum B_n \ddot{\xi}_n \quad (3.16)$$

where

$$A_n = \int_0^L [v_n(t)]^2 ds \quad (3.17)$$

and

$$B_n = \int_0^L t v_n(t) ds \quad (3.18)$$

Here, of course, all forces and masses are understood to be per unit length of the canal.

It is important to note that for the circular canal these results are valid without the restriction imposed in the general development that only rectilinear motion of the tank in the x direction was permitted. Rotation of the canal about its center produces no sloshing, nor, by symmetry, does vertical tank motion produce horizontal sloshing force. (In fact, it can be shown that vertical motion produces no sloshing at all in the circular canal.) Since all pressures are in a radial direction, the resultant horizontal slosh force F_S always passes through the center of the canal.

3.2 SPHERICAL TANK

In terms of the sloshing natural modes $\psi_n = \psi_n(r, \theta) \cos k\theta$, the parameter β_n is

$$\beta_n = \frac{a_n^2}{g} \int_0^{aR} \int_0^{2\pi} r(r \cos \theta) \psi_n(r, \theta) \cos k\theta dr d\theta$$

Thus, it follows that β_n vanishes for all $k \neq 1$, justifying the restriction previously made to consideration of only the case $k = 1$. The values of ψ_n at the free surface are proportional to $f_n(\rho)$, where $f_n(\rho) = \frac{1}{\sqrt{\rho}} g_n(\rho)$, and $g_n(\rho)$ is an eigenfunction of the integral equation (2.28). Normalize $f_n(\rho)$ so that $f_n(1) = 1$. Then, as in the circular-canal case, the slosh height ξ_n at the wall is $a_n \omega_n^2/g$, and

$$\beta_n = (aR)^3 \frac{\omega_n^2}{g} \int_0^{2\pi} \int_0^1 \rho^2 f(\rho) \cos^2 \theta d\rho$$

$$= \pi (aR)^3 \frac{\omega_n^2}{g} \int_0^1 \rho^2 f(\rho) d\rho$$

$$\alpha_n = (aR)^2 \int_0^{2\pi} \int_0^1 \rho [f(\rho)]^2 \cos^2 \theta d\rho$$

$$= \pi (aR)^2 \int_0^1 \rho [f(\rho)]^2 d\rho$$

Hence, from Eqs. (3.11) - (3.13),

$$\ddot{\xi}_n + \omega_n^2 \xi_n = - (\lambda_n a) \left(\frac{D_n}{C_n} \right) \ddot{U} \quad (3.19)$$

$$(M_c + M_L) \ddot{U} + \pi \rho_L (aR)^3 \sum D_n \ddot{\xi}_n = X \quad (3.20)$$

$$F_S = - M_L \ddot{U} - \pi \rho_L (aR)^3 \sum D_n \ddot{\xi}_n \quad (3.21)$$

where

$$c_n = \int_0^1 \rho [f_n(\rho)]^2 d\rho = \int_0^1 [g_n(\rho)]^2 d\rho \quad (3.22)$$

and

$$d_n = \int_0^1 \rho^2 f_n(\rho) d\rho \quad (3.23)$$

The force F_g , again, passes through the center of the sphere.

Section 4
NUMERICAL RESULTS

4.1 CIRCULAR CANAL

The first three modes and frequencies for the circular canal were found for the values $e = 1, 0.8, 0.6, 0.4, 0.2, 0, -0.2, -0.4, -0.6$, and -0.8 , from the 20-by-20 matrix formulation described in Appendix A. The values of $(\lambda_1 a)$ and λ_n ($n = 1, 2, 3$) thus obtained, together with those found analytically for $e = -1$, are given in Table 4-1.

The solid curves in Fig. 4-1 show the variation with e of $\sqrt{\lambda}$ (which is proportional to frequency) for the first three modes. Worthy of note is the fact that the variation with e of the higher frequencies is not monotonic; the minimum frequency of a given higher mode appears to occur slightly below the half-full condition, whereas the fundamental mode has its lowest frequency in the nearly-empty state. This situation is at least partially associated with the fact that, in general, as depth increases, frequencies of free-surface oscillation tend to shift to more closely packed spectra. Thus, for example, the ratio λ_2/λ_1 decreases monotonically with increasing e .

For the nearly-full case ($e = 1$) the matrix calculation provided the result $(\lambda_1 a) = 2.018$, as compared with the upper bound of 2.094 obtained from the one-term Galerkin solution. The corresponding asymptotic behavior

$$\sqrt{\lambda_1} \approx \frac{(2.018)^{1/2}}{(1-e^2)^{1/4}} \quad \text{for } e \rightarrow 1$$

is shown as the dotted curve in Fig. 4-1; the asymptotic behaviors for $\sqrt{\lambda_2}$ and $\sqrt{\lambda_3}$ are similarly indicated.

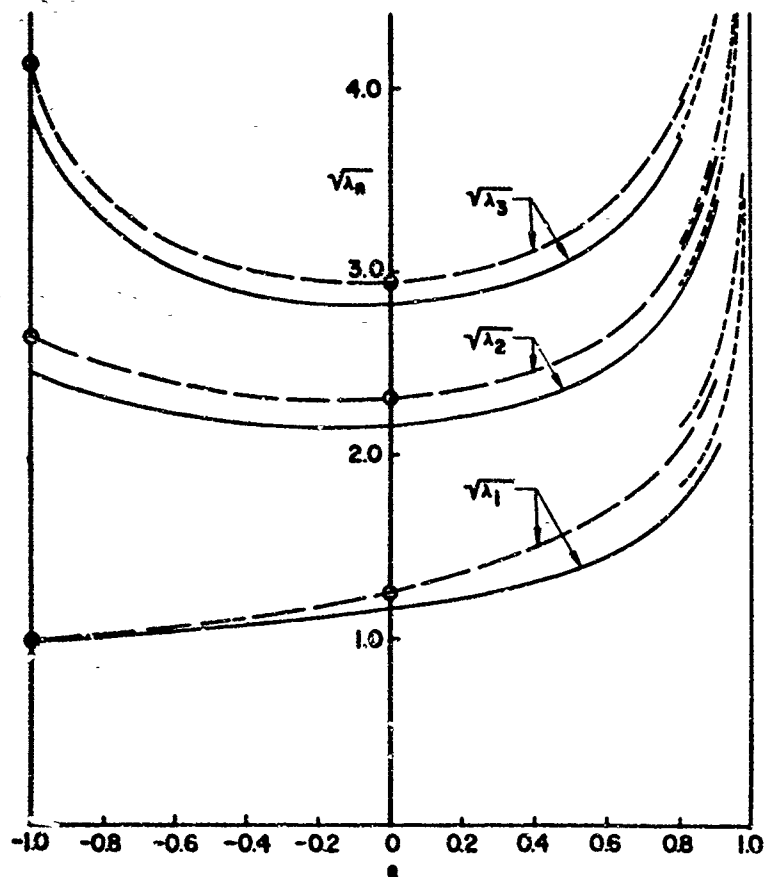


Fig. 4-1 Frequencies for Circular Canal

4-2

It may be noted that the upper bound $\lambda_1 = 1.367$ obtained by Rayleigh (or by the one-term Galerkin solution of this paper) for the half-full canal is very close to the value $\lambda_1 = 1.360$ found from the matrix calculation. Rayleigh's improved upper bound, corresponding to $\lambda_1 = 1.356$, is actually more accurate, but there is little doubt that the results obtained from the matrix set-up are entirely satisfactory for practical application.

The modal parameters A_n and B_n defined by Eqs. (3.16) and (3.17) are plotted against e in Fig. 4-2. Except for the nearly-empty case ($e = -1$), these parameters were found by numerical integration. For $e = -1$, the result (Eq. [2.22]) for the natural mode shapes provides:

$$\begin{aligned} A_n &= \frac{1}{4n-1} \\ B_n &= 1/3 \text{ for } n = 1 \\ &= 0 \text{ for } n > 1 \end{aligned}$$

The modal parameter B_n is closely related to the amount of n^{th} mode induced by lateral acceleration. The low values of B_n for $n > 1$ indicate that, in general, the higher modes would not have a major influence on sloshing forces.

The mode shapes $w_n(\xi)$ are shown in Fig. 4-3 for $e = 1, 0$, and -1 . A point of minor theoretical interest in connection with the mode shapes is that the slope at $\xi = 1$ can be shown to be given by

$$w_n'(1) = -\lambda_n e$$

Thus, the slope is negative for $e > 0$ and positive for $e < 0$; for $e = 1$, the slope is infinite. The nature of these slopes is a direct consequence of the inclination of the container wall at the free surface.

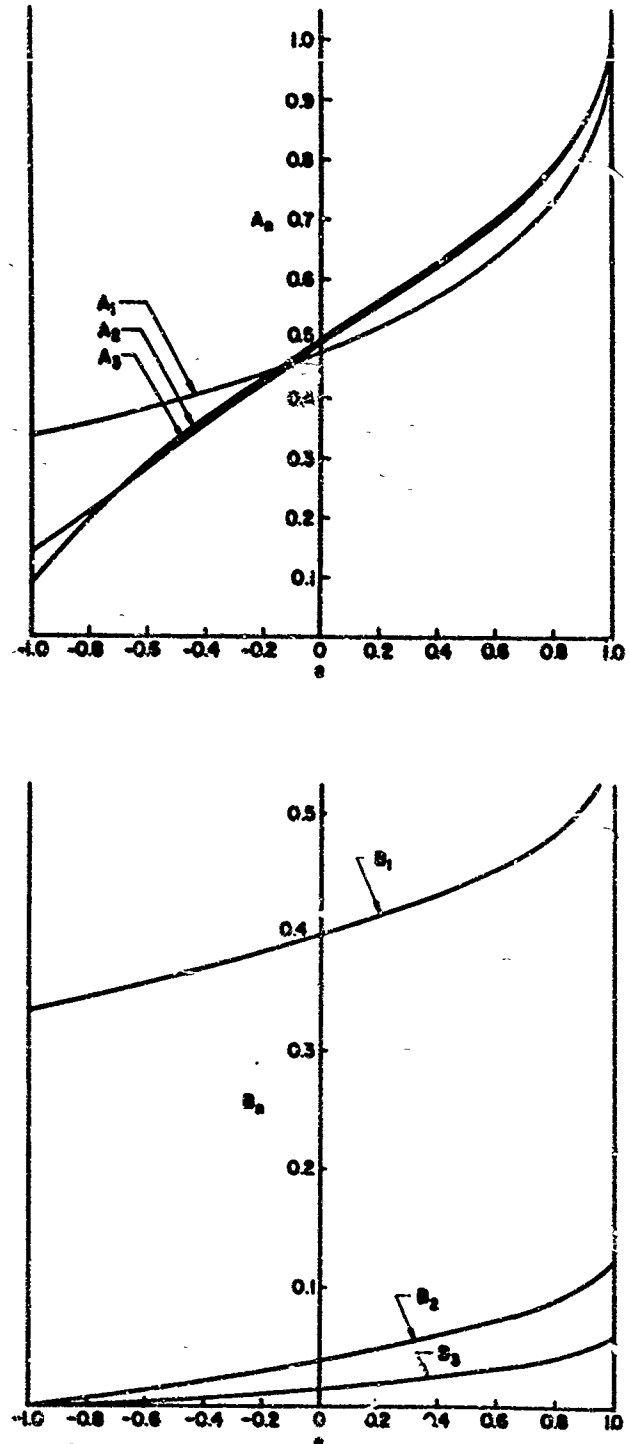


Fig. 4-2 Modal Parameters for Circular Canal

4-4

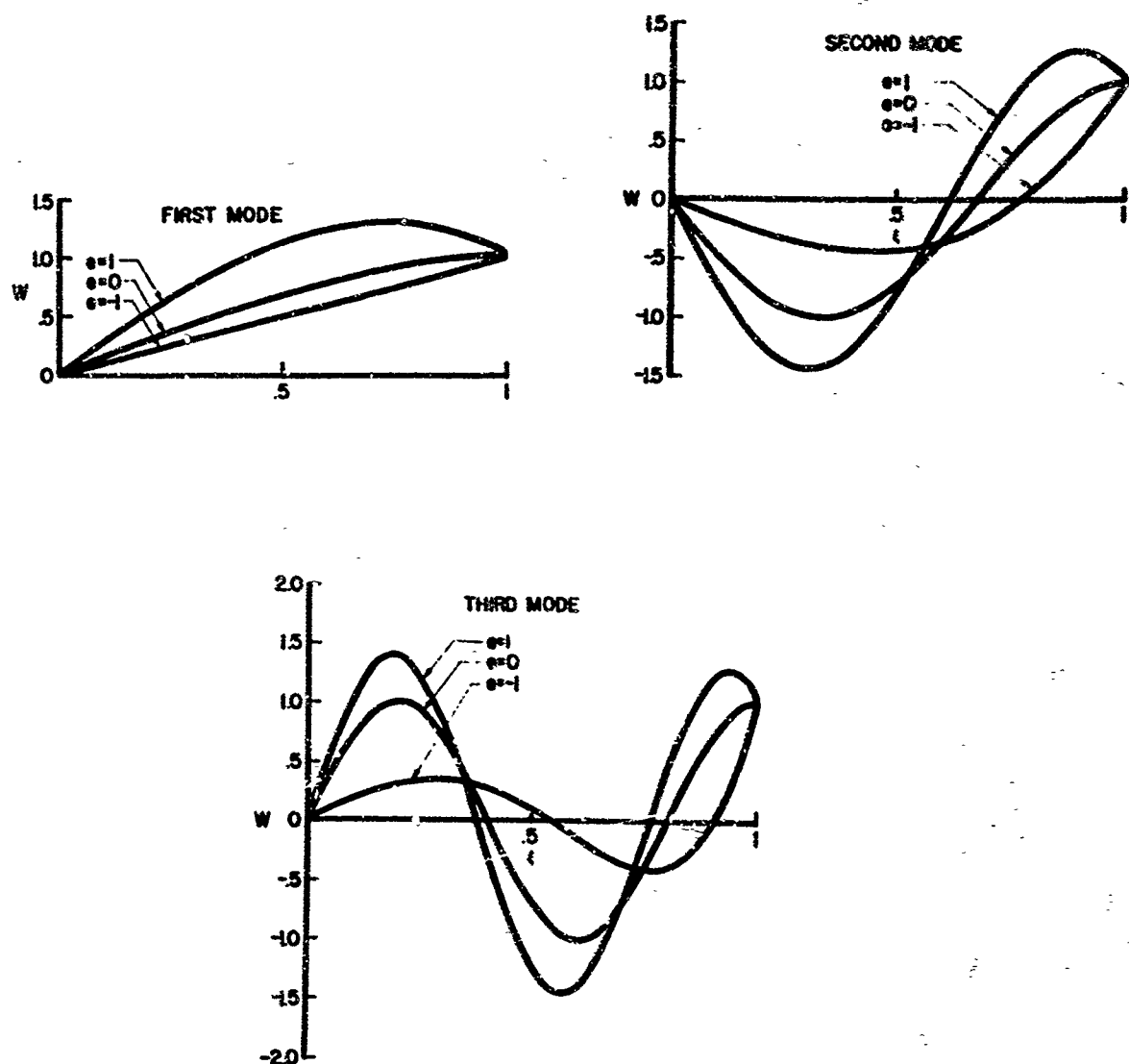


Fig. 4-3 Mode Shapes for Circular Canal

4.2 SPHERICAL TANK

The values of $(\lambda_n a)$ and λ_n for the nearly-full ($e = 1$) and half-full ($e = 0$) spherical tank were found, for $n \geq 1, 2$, and 3 , from the matrix formulation described in Appendix A and are given in Table 4.2. Also presented in this table are the values found analytically for the nearly empty tank ($e = -1$). From the values of $(\lambda_n a)$ for $e = 1$, the asymptotic behavior of $\sqrt{\lambda_n}$ near $e = 1$ is shown as the dot-dash curves in Fig. 4-2, and the values of $\sqrt{\lambda_n}$ for $e = 0$ and $e = 1$ are shown as the circles in this figure. The dashed curves represent estimates of the variation of λ_n in the intermediate ranges, based on the presumably analogous trends for the circular canal.

The modal parameters C_n and D_n were calculated (by numerical integration for $e = 1$ and $e = 0$, and analytically from Eq. 2.42 for $e = -1$) and are shown in Fig. 4-4. The curves connecting the calculated points in this figure were estimated, with the results of Fig. 4-1 for the canal as a guide.

Finally, the mode shapes $f_n(\rho) = \frac{1}{\sqrt{\rho}} g_n(\rho)$ for the three calculated cases are given in Fig. 4-5.

TABLE 4-1

EIGENVALUES FOR CIRCULAR CANAL

e	a	λ_1^a	λ_2^a	λ_3^a	λ_1	λ_2	λ_3
-1.0	0.0	0.0	0.0	0.0	1.0	6.0	15.0
-0.8	0.6	0.627	3.23	6.51	1.045	5.38	10.85
-0.6	0.8	0.879	3.98	7.30	1.099	4.97	9.13
-0.4	0.917	1.068	4.34	7.63	1.165	4.74	8.33
-0.2	0.980	1.224	4.56	7.82	1.249	4.65	7.99
0.0	1.0	1.360	4.70	7.96	1.360	4.70	7.96
0.2	0.980	1.482	4.81	8.05	1.513	4.91	8.23
0.4	0.917	1.596	4.89	8.15	1.742	5.34	8.89
0.6	0.8	1.706	4.97	8.22	2.13	6.22	10.28
0.8	0.6	1.822	5.05	8.30	3.04	8.42	13.84
1.0	0.0	2.018	5.20	8.44	∞	∞	∞

TABLE 4-2

EIGENVALUES FOR SPHERICAL TANK

e	a	λ_1^a	λ_2^a	λ_3^a	λ_1	λ_2	λ_3
.1	0.0	0.0	0.0	0.0	1.0	7.0	17.0
0	1.0	1.565	5.34	8.66	1.565	5.34	8.66
1	0.0	2.78	5.99	9.25	∞	∞	∞

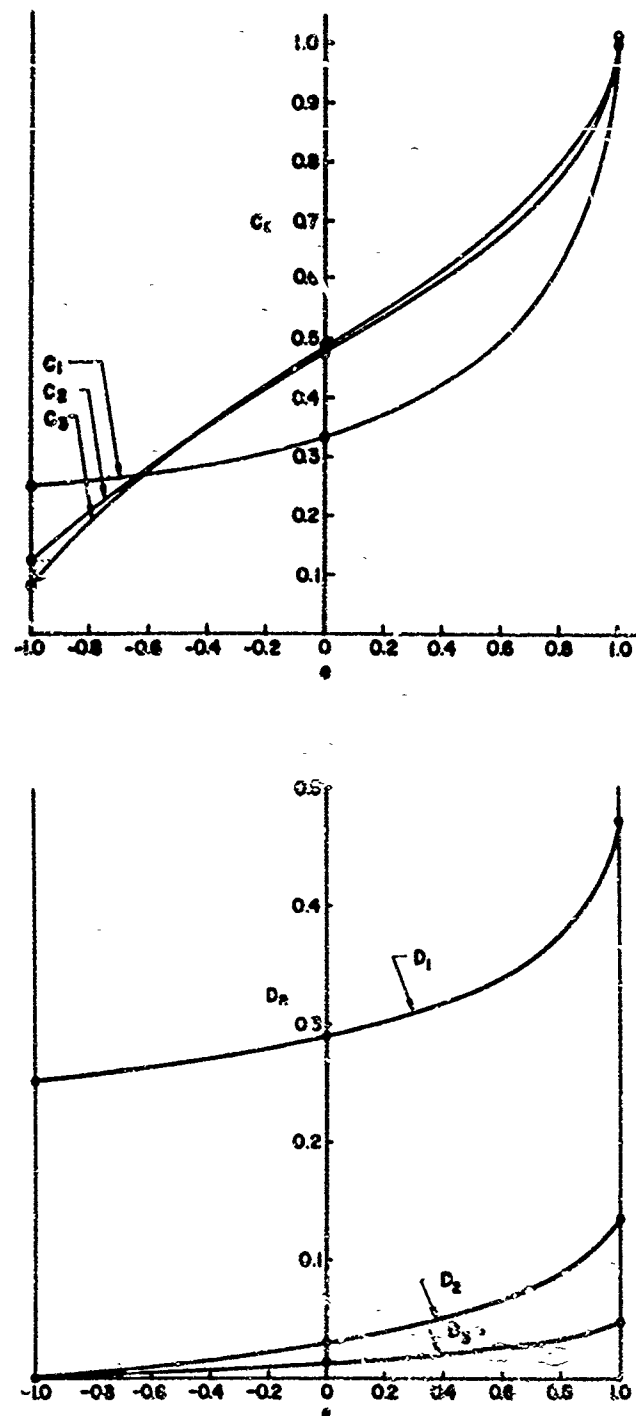


Fig. 4-4. Modal Parameters for Spherical Tank

4-8

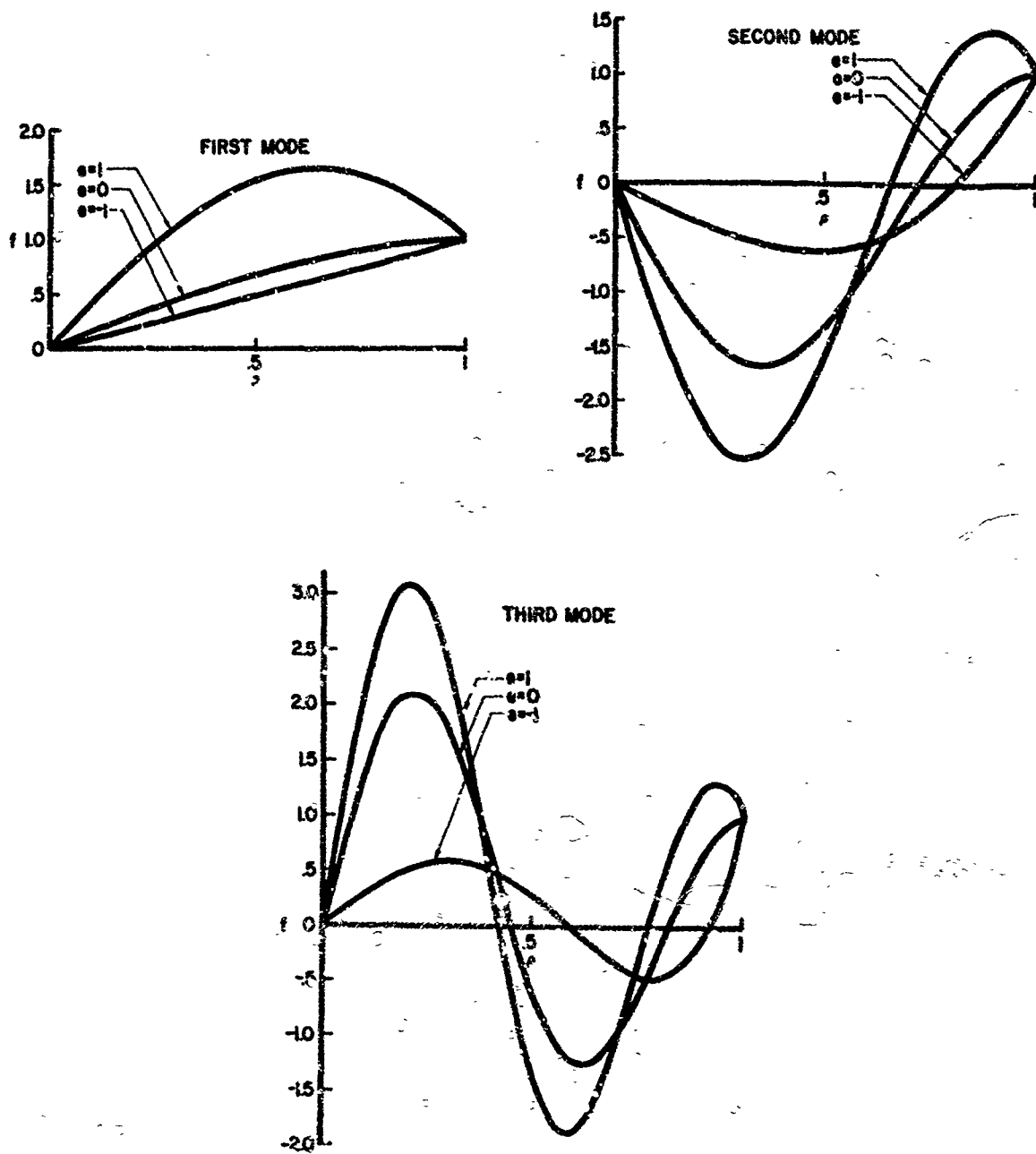


Fig. 4-5 Node Shapes for Spherical Tank

4-9

Section 5
COMPARISON WITH EXPERIMENT

Resonance tests (unpublished) conducted by the Lockheed Missile Systems Division on partially filled spherical tanks provided the experimental results for $\sqrt{\lambda_1}$, which are shown as crosses in Fig. 5-1. The estimated curve for $\sqrt{\lambda_1}$ given in Fig. 4-2 is reproduced in Fig. 5-1 for comparison. The agreement is generally good, and the agreement of experiment with the rigorously calculated frequency for the half-full case is excellent.

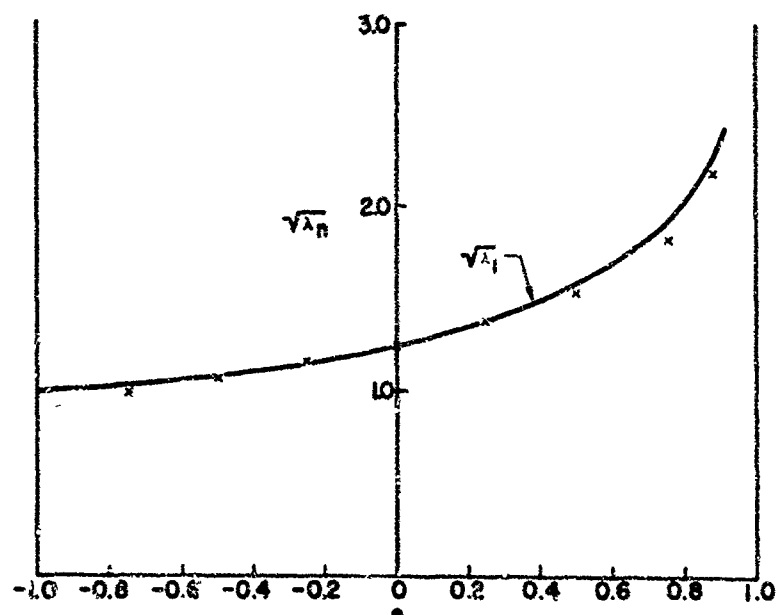


Fig. 5-1 Experimental Frequencies for Spherical Tank

5-1

Section 6
CONCLUSIONS

The results for the circular canal are sufficiently complete to be used in the dynamic analysis of such canals filled to arbitrary depth. Some degree of caution is evidently required, however, in the use of the estimated results for the spherical tank in the ranges intermediate to the nearly-empty, half-full, and nearly-full cases.

6-1

Section 7
REFERENCES

1. Lamb, Sir Horace, Hydrodynamics, 6th ed., Dover Publications, New York, 1945.
2. Douglas Aircraft Company, The Forces Produced by Fuel Oscillation in a Rectangular Tank, by E. W. Graham, SM-13748, Apr 1951
3. Remo-Wooldridge Corporation, Variational Solution of Fuel Sloshing Modes, by H. R. Lawrence, C. T. Wang, and R. B. Reddy, Dec 1957
4. Jahnke, E. and F. Emde, Tables of Functions, 4th ed., Dover Publications, New York, 1945
5. Grobner, W. and N. Hofreiter, Integraltafel, Zweiter Teil, Bestimmte Integrale, Springer-Verlag, Vienna, 1950, p. 40
6. Kellogg, O. D., Foundations of Potential Theory, Ungar Publishing Co., New York, n.d., p. 247
7. Byrd, Paul F. and Morris D. Friedman, Handbook of Elliptic Integrals, Springer-Verlag, Berlin, 1954

7-1

Appendix A
NUMERICAL SOLUTION OF INTEGRAL
EQUATIONS

The general kernel function (Eq. [2.13]) for the circular canal has a logarithmic singularity at $\xi = \bar{\xi} > 0$. For ξ near $\bar{\xi}$, with $\xi \neq 1$,

$$G(\xi, \bar{\xi}) \approx -\frac{1}{\pi} \log |\xi - \bar{\xi}| + p(\xi) \quad (\text{A.1})$$

where

$$p(\xi) = -\frac{1}{\pi} \log \left\{ \frac{2\gamma (1-\xi)^{2\gamma-1}}{(1+\xi)^{2\gamma} - (1-\xi)^{2\gamma}} \right\} \quad (\text{A.2})$$

Near $\xi = 1$,

$$G(1, \bar{\xi}) \approx -\frac{2}{\pi} \log |1 - \bar{\xi}| + \gamma \log 2 \quad (\text{A.3})$$

Note, however, that $G(0, \bar{\xi}) = G(\xi, 0) = 0$, and recall that $w(0) = 0$.

Then the integral

$$\int_0^1 G(\xi, \bar{\xi}) w(\bar{\xi}) d\bar{\xi}$$

may be approximated by

$$\sum_{i=1}^{N-1} \omega(i\Delta) \int_{1-\frac{\Delta}{2}}^{1+\frac{\Delta}{2}} G(\xi, \bar{\xi}) d\bar{\xi} \approx w(1) \int_{1-\frac{\Delta}{2}}^1 G(\xi, \bar{\xi}) d\bar{\xi} \quad (\text{A.4})$$

where $\Delta = \frac{1}{N}$. Suppose $t = j\Delta$; then

$$\int_{j\Delta - \frac{\Delta}{2}}^{j\Delta + \frac{\Delta}{2}} G(t, \bar{t}) d\bar{t} \approx \Delta G(j\Delta, j\Delta) \quad j \neq N$$

$$\int_{1 - \frac{\Delta}{2}}^1 G(t, \bar{t}) d\bar{t} \approx \frac{\Delta}{2} G(j\Delta, 1) \quad j \neq N$$

$$\begin{aligned} \int_{j\Delta - \frac{\Delta}{2}}^{j\Delta + \frac{\Delta}{2}} G(t, \bar{t}) d\bar{t} &\approx \Delta p(j\Delta) + \int_{-\frac{\Delta}{2}}^{\frac{\Delta}{2}} -\frac{1}{\pi} \log |t| dt \\ &= \Delta \left[p(j\Delta) + \frac{1}{\pi} \left(1 - \log \frac{\Delta}{2} \right) \right] \quad j \neq N \end{aligned}$$

$$\int_{1 - \frac{\Delta}{2}}^1 G(1, \bar{t}) d\bar{t} \approx \frac{\Delta}{2} \left[\left(\frac{1}{\pi} \log 2 \right) + \frac{1}{\pi} \left(1 - \log \frac{\Delta}{2} \right) \right]$$

Hence, the integral equation (2.14) is approximated by the matrix equation

$$A T \{w\} = \left(\frac{N}{\lambda a} \right) \{w\} \quad (A.5)$$

where $\{w\}$ is the column vector with elements $w(j\Delta)$ ($j = 1, 2, \dots, N$), T is the "integrating" diagonal matrix $\begin{bmatrix} 1 & & & \\ & 1 & & \\ & & \ddots & \\ & & & 1 \end{bmatrix}$, and A is the symmetrical

$$\begin{bmatrix} 1 & & & \\ & 1 & & \\ & & \ddots & \\ & & & 1 \end{bmatrix}$$

square matrix with the general element A_{ij} defined by:

$$A_{ij} = G(i\Delta, j\Delta) \quad i \neq j \neq N$$

$$= p(j\Delta) + \frac{1}{\pi} (1 - \log \frac{\Delta}{2}) \quad i = j \neq N$$

$$= \frac{1}{\pi} \log 2 + \frac{1}{\pi} (1 - \log \frac{\Delta}{2}) \quad i = j = N$$

Note that, in the absence of a logarithmic singularity, the integration scheme would reduce precisely to the conventional trapezoidal rule.

The orthogonality condition for distinct eigenfunctions w_m and w_n

$$\int_0^1 w_m(\xi) w_n(\xi) d\xi = 0$$

is approximated, according to trapezoidal rule, by

$$[w_m]^T [w_n] = C \quad (A.6)$$

where $[w_m]$ is a row matrix and $[w_n]$ is a column matrix.

The orthogonality condition (Eq. A.6) is satisfied exactly by the eigenvectors of the matrix equation (A.5), and, for this reason, the present integration scheme is considered to be a reasonably appropriate one.

An entirely analogous scheme is adaptable to the integral equation (2.22) for the spherical tank. In the case of the nearly-full tank, the behavior of $H(\rho, \bar{\rho})$ near $\bar{\rho} = \rho$ is

$$H(\rho, \bar{\rho}) \approx -\frac{1}{\pi} \log |\rho - \bar{\rho}| + \frac{1}{\pi} (\log \rho + \log 8 - 2). \quad (A.7)$$

including the case $\rho = 1$.

A-3

For the half-full tank, for $\bar{\rho}$ near ρ , with $\rho \neq 1$,

$$H(\rho, \bar{\rho}) \approx -\frac{1}{\pi} \log |\rho - \bar{\rho}| + \frac{1}{\pi} [\log \rho + 2\rho^3 K(\rho^2) + \log 8 - 2] \quad (A.8)$$

On the other hand, $H(1, \bar{\rho})$ near $\bar{\rho} \approx 1$ is

$$H(1, \bar{\rho}) \approx -\frac{2}{\pi} \log (1 - \bar{\rho}) + \frac{1}{\pi} (2 \log 8 - 2) \quad (A.9)$$

Hence, the matrix formulations for the spherical tank may be made in a fashion similar to those for the circular canal; the eigenvectors are then proportional to $\sqrt{\rho f_n(\rho)}$.

Eigenvalues and eigenvectors of the matrix $C = AT$ (Eq. [A.5]) were found by using a Remington Rand 1103AF computer on the basis of 20-by-20 matrix approximation (i.e., $N = 20$). The highest eigenvalue of C (and hence the lowest value of λ) and the corresponding eigenvector were found by matrix iteration. The second mode was found from the modified ("swept") matrix

$$C' = C - C [w_1] [w_1]^T$$

where w_1 is the previously determined first eigenvector, normalized according to

$$[w_1]^T [w_1] = 1$$

After determining the second eigenvalue and eigenvector, again by iteration, C' was similarly swept to provide a matrix C'' , direct iteration of which gave the third eigenvalue and eigenvector.

A-4